# Experimental wavelengths for intrashell transitions in tungsten ions with partially filled $3p$ and $3d$ subshells

Thomas Lennartsson
*Lund Observatory, Box 43, SE-221 00 Lund, Sweden*

Joel Clementson* and Peter Beiersdorfer†
*Lawrence Livermore National Laboratory, Livermore, California 94550, USA*

(Received 12 February 2013; published 14 June 2013)

Spectra and measured wavelengths of intrashell $n = 3$ transitions in highly charged tungsten ions with partially filled $3p$ and $3d$ valence shells, Al-like $W^{61+}$ through Fe-like $W^{48+}$, are presented. The ions were created and excited at the electron-beam ion-trap facility at the Lawrence Livermore National Laboratory and measured with a high-resolution grazing-incidence spectrometer. The spectral lines were studied in the 27–41 Å range and were analyzed by a comparison with synthetic spectra based on a collisional-radiative model. We determined that the emission includes not only electric-dipole-allowed transitions, but also several electric-quadrupole and magnetic-dipole transitions. Line-position uncertainties as low as 25 ppm were achieved. Thus, our measurements provide much-needed benchmarks for calculations of the atomic structure of highly charged ions with a partially filled subshell, since these ions are difficult to calculate due to electron-correlation effects.

DOI: 10.1103/PhysRevA.87.062505 PACS number(s): 32.30.Jc, 31.15.V−, 31.30.jf

## I. INTRODUCTION

The investigation of tungsten ions is of great importance in both theoretical and applied atomic physics. Relativistic and quantum electrodynamical effects depend strongly on $Z$ [1,2] and are thus necessary to include when modeling high-$Z$ systems. For multielectron, high-$Z$ ions, such as the tungsten ions with $3p$ and $3d$ valence electrons (Al-like $W^{61+}$ through Ni-like $W^{46+}$), correlation effects dominate most of the remaining uncertainty in atomic calculations [3,4]. In recent years atomic theory has seen improvements in the treatment of correlations as calculational tools evolved from early multiconfiguration Dirac-Fock (MCDF) structure codes with a limited number of levels in a given basis set [5,6] to relativistic configuration-interaction calculations [3,4] with $10^5$ and more interacting levels and to the use of relativistic many-body perturbation theory (RMBPT) [7,8] and the multireference Møller-Plesset approach [9,10], which treats correlations up to second order. High-precision measurements of the $3p$-$3d$ and $3p$-$3p$ transition wavelengths in tungsten ions are thus of importance since they can be used as benchmarks for advancing electron-correlation physics in multielectron, high-$Z$ ions.

Spectral observations of $3p$-$3p$ and $3p$-$3d$ transitions are also of great interest because they can reveal electric-dipole-forbidden transitions. Forbidden transitions are important for plasma diagnostics because they are sensitive to the electron density, and numerous electric-dipole-forbidden transitions have recently been identified in various charge states of tungsten [11–13]. For example, Ralchenko *et al.* [14] have identified about three dozen $3d$-$3d$ magnetic dipole transitions in the 120–220 Å range from Co-like $W^{55+}$ through K-like $W^{47+}$ from spectra recorded at the National Institute of Standards and Technology (NIST) electron-beam ion trap. Forbidden transitions have generally much smaller radiative rates than electric-dipole-allowed transitions, and they are, thus, also important candidates for measurements of radiative rates using ion traps and storage-ring methods [15,16].

The interest in tungsten spectroscopy in applied physics is due to its potential use in plasma diagnostics in the future tokamak fusion reactor ITER [17–19]. Between approximately 10 and 60 Å the strongest tungsten emission is expected to be due to $n = 3$ to $n = 3$ transitions in the $M$-shell ($n = 3$) ions [20–22], and spectroscopic data in this region are important in order to monitor the tungsten-ion impurity levels and to properly predict the radiative emission. Of special interest is the mapping of high-order multipole transitions, such as magnetic-dipole ($M1$) or electric-quadrupole ($E2$) transitions. The long-lived metastable levels, from which electric-dipole-forbidden transitions proceed, are important for a correct description of the ionization balance, as metastable levels will effectively act as ground levels from which the ion can reach its next charge state through electron collisions. In addition, measuring the line intensity ratios between electric dipole ($E1$) and high-order multipole transitions in the fusion plasmas may be used to complement other methods for determining electron densities in ITER, as previously discussed by Ralchenko *et al.* [14].

A number of theoretical studies of $M$-shell transition energies in few-electron systems like Na-like $W^{63+}$ and Mg-like $W^{62+}$ have been made. Because of their complexity and the associated computational challenge, rather few calculations have been made involving a higher number of electrons. Excitation energies in the Al isoelectronic sequence were calculated by Huang [23] using the relativistic multiconfiguration Hartree-Fock (MCHF) technique and with the RMBPT method by Safronova *et al.* [24]. RMBPT was also used by Safronova and Safronova [25] to calculate wavelengths and transition rates for intershell transitions in a number of tungsten ions, among them Al-like $W^{61+}$ and Ca-like $W^{54+}$. Chen and Cheng [26] calculated transition energies in Ne-like $W^{64+}$

*Present address: Max Planck Institute for Plasma Physics, EURATOM Association, DE-17491 Greifswald, Germany
†beiersdorfer1@llnl.gov

 

through Si-like $W^{60+}$ and in Ar-like $W^{56+}$ using the RCI code. Calculations with the MCHF technique on Si- through Cl-like ions, including tungsten, were made by Huang [27,28], Chou *et al.* [29], and Huang *et al.* [30]. Quinet [31] recently used a fully relativistic Dirac-Fock method to compute wavelengths and transition probabilities for forbidden lines in Al-like $W^{61+}$ through Co-like $W^{47+}$. Transition wavelengths for Co-like $W^{47+}$ were among a number of lower charge states calculated by Fournier [32] using the ANGLAR and RELAC codes. In addition, the $3l$-$4l$ spectra of several $M$-shell ions were recently calculated by Clementson *et al.* [33] using the Flexible Atomic Code (FAC).

Few experimental studies of $M$-shell tungsten ions are available to guide theory and distinguish among different approaches for calculating open $3p$- and $3d$-shell ions. Ralchenko *et al.* [34] measured spectra in Na-like $W^{63+}$ through Ca-like $W^{54+}$ in the 40–200 Å region using the electron-beam ion trap located at NIST. Later, 37 previously unknown $M1$ transitions in K-like $W^{55+}$ through Co-like $W^{47+}$ between 100 and 250 Å were reported by Ralchenko *et al.* [14]. Several of these lines were suggested to be used in line ratios to measure the electron density in fusion plasmas. The spectra of Ne-like $W^{64+}$ through K-like $W^{55+}$ were studied between 19 and 25 Å by Clementson and Beiersdorfer [35] using the high-energy SuperEBIT at the Lawrence Livermore National Laboratory (LLNL). In addition, Clementson *et al.* [36] measured the $3l$-$4l'$ spectra from Co-like $W^{47+}$ and a number of lower charge states with transition wavelengths in the 3.4–8.3 Å range. The precision of these measurements is typically between 200 and 500 ppm, with 140 ppm at best. An exception of 30 ppm was achieved by Utter *et al.* [37], where an optical $M1$ transition in Ti-like $W^{52+}$ was measured using the Livermore EBIT-II electron-beam ion trap.

In the present paper, we report on wavelengths of $3p$-$3p$ and $3p$-$3d$ transitions in Al- through Co-like W measured between 27 and 41 Å at the Livermore EBIT-I electron-beam ion trap using a high-resolution grazing-incidence spectrometer. The typical precision is better than 100 ppm, with several lines between 25 and 30 ppm, which is very high for highly charged tungsten ions with open $3p$ and $3d$ shells. For line identification, atomic structure and line intensity calculations were made using FAC [38,39].

## II. THEORY

The structure and spectra of the 18 $M$-shell tungsten ions isoelectronic to Na ($W^{63+}$) through Ni ($W^{46+}$) were calculated using the Flexible Atomic Code v1.1.1., written by Gu [38,39]. FAC is a suite of codes for relativistic atomic structure calculations suitable for highly charged ions. Using a modified single potential, the atomic state functions are calculated from a Dirac-Fock-Slater iteration and Dirac-Coulomb Hamiltonian. Continuum processes are treated using the distorted-wave approximation.

The ions were modeled in a frozen-core approximation. For Na-like through Ca-like W the $K$ shell was held closed and for Sc-like through Ni-like W also the $L$ shell. The number of configuration state functions used in the structure calculations depended on the atomic complexity: for the $3s$ and $3p$ ions plus the K- and Ca-like W ions configurations with singly excited $L$-shell electrons were included in addition to singly and also several multiply excited $M$-shell electron configurations. The lower charge states had all the singly excited and many multiply excited configuration state functions. All ions were modeled with configurations having a single electron in the $n = 4$ and 5 shells. Mn- through Ni-like W furthermore included a single electron in the $n = 6$ shell. Autoionization was calculated for Na- through Ca-like W, where all autoionization channels to the ground, and some low-excited levels depending on the ion, of the daughter ion were included. Collisional electron excitation and deexcitation were calculated between the ground and low-excited levels to all levels. Radiative decays were considered between all levels in the systems. The spectra were modeled for $N_e = 5 \times 10^{12}$ cm$^{-3}$, $E_b = 18.2$ keV, and $\Delta E_b = 30$ eV with Gaussian line distributions of 25 mÅ full width at half maximum.

## III. MEASUREMENT AND ANALYSIS

The experiment was performed at the LLNL electron beam ion trap facility [40,41], where tungsten was injected into EBIT-I by sublimation of tungsten hexacarbonyl $W(CO)_6$. The atoms were ionized by being exposed to an electron beam with an energy of 18.2 keV, current of 200 mA, and width $\leqslant 60$ $\mu$m. The spectrometer used was a flat-field grating spectrometer for high-resolution soft x-ray and extreme ultraviolet measurements [42]. The electron beam is dispersed and directly imaged onto the detector through a variable-line-spaced grating with a nominal line density of 2400 lines/mm, a radius of curvature of 44.3 m, and a grazing-incidence angle of $\sim 2^\circ$. The spectra were recorded using a back-illuminated Princeton Instruments charge-coupled device (CCD) detector, cooled with liquid nitrogen. The CCD consists of a $1300 \times 1340$ array, each pixel of size $20 \times 20$ $\mu$m$^2$. The widths of the spectral lines imaged on the detector were slightly above 3 pixels, which, for a 60 $\mu$m beam, is close to best focus.

To calibrate the wavelength scale of the tungsten spectra, carbon dioxide was supplied to the trap by gas injection. Reference spectra of carbon and oxygen ions were recorded and a second-order polynomial of wavelength versus pixel position was fitted by using theoretical transition wavelengths. The polynomial was anchored to C V lines also present in the tungsten spectra. The Ly-$\alpha$, Ly-$\beta$, and Ly-$\gamma$ lines in C VI and the Ly-$\alpha$ lines in O VIII were taken from the work of Garcia and Mack [43], the $K\alpha$ $w$ lines in C V and O VII were from Drake [44], and the $K\beta$ transition in C V was from Vainshtein and Safronova [45].

The spectrometer was set up to record spectra at two positions, the first covering the 26.5–35.0 Å range and the second the 33.0–43.5 Å range. The tungsten spectra were recorded in batches of (4–8) $\times$ 30 min exposures over the course of several days; each batch (where all 30 min exposures were added) was calibrated with carbon- and oxygen-ion spectra before and after exposure. The recorded images were rotated to compensate for a small tilt in the camera setup and filtered for cosmic-ray contamination. The summed intensity of all batches for the two different ranges is presented in Figs. 1 and 2.

When analyzing each calibration spectrum separately, it was found that the calibration lines were moving slightly on the CCD array during the course of the day, most likely

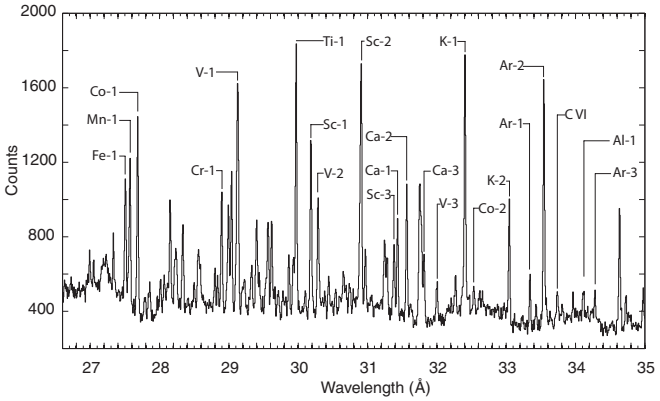


FIG. 1. EBIT-I spectrum of highly charged tungsten recorded in the 26.5–35.0 Å range at a beam energy of 18.2 keV.

due to small temperature variations, since the displacement in line position was smooth with a period of ∼24 h. Each batch was therefore calibrated with the mean positions of the calibration lines before and after recording the tungsten-ion spectra. The uncertainties associated with the drift of the lines and the counting statistics were estimated by measuring the line positions in each batch, averaging, and calculating the standard deviations weighted by the signal-to-noise ratio for each line. This uncertainty ranges typically from below 1 mÅ for strong lines to 4 mÅ for weaker ones. The analysis of the calibration spectra is also afflicted by uncertainties. The uncertainties in the theoretical wavelengths themselves are hard to estimate, and we have assumed the experimental uncertainties of He-like ion measurements by Engström and Litzén [46]. This typically gives a contribution of 0.2 mÅ. The uncertainty in the polynomial fitting routine is found to add another 0.1–0.5 mÅ, while the counting-statistics contribution for the carbon- and oxygen-ion line positions is so small in comparison to the other uncertainties that it can be neglected. All these uncertainties have been added in quadrature and result in total wavelength uncertainties between 0.7 and 10 mÅ.

When no ions, atoms, or molecules are purposely supplied to EBIT, barium ($Z = 56$), which originates from the electron gun filament, typically constitutes the dominant trapped species [47]. The electron gun also contains other elements, most notably tungsten ($Z = 74$), which also emanates from the

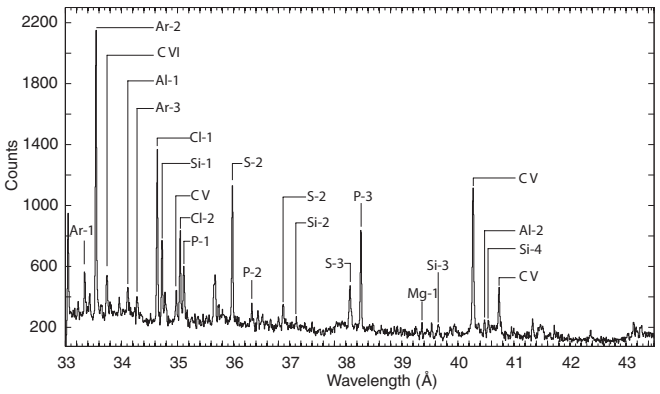


FIG. 2. EBIT-I spectrum of highly charged tungsten recorded in the 33.0–43.5 Å range at a beam energy of 18.2 keV.

gun filament but at a slower rate than barium, and then takes over as the dominant species in the trap. The reason is that heavier ions, such as tungsten, are trapped preferentially over lighter ions, which simply serve to cool the heavier ions [48]. When injecting $W(CO)_6$, tungsten dominates, and the lighter ions of carbon and oxygen act as light-ion coolants. The high number of carbon ions continuously injected, however, enabled the strongest of the carbon lines to appear in the spectra (see Figs. 1 and 2). The presence of lines from any other impurities, such as barium, is, however, unlikely because the slow rate with which such impurities enter the trap is overpowered by the fast rate at which $W(CO)_6$ is injected.

To identify the lines, a synthetic spectrum was calculated for an electron energy of 18.2 keV, an electron density of $5 \times 10^{12}$ cm$^{-3}$, and with linewidths of 0.025 Å. The constants used to convert the calculated transition energies to wavelengths were $h = 6.626\,069\,57 \times 10^{-34}$ J s, $c = 2.997\,924\,58 \times 10^{8}$ ms$^{-1}$, and $e = 1.602\,176\,565 \times 10^{-19}$ C [49]. When comparing identified lines with the wavelengths calculated by FAC, the largest differences (∼0.15 Å) are, as expected, found in the ions with the highest number of electrons, where correlation effects peak. This makes it more difficult to use FAC for identification towards shorter wavelengths where the emission from the lowest charge states is found. Especially complex regions are 27.70–28.70 and 29.20–29.80 Å, where a number of moderately intense lines are measured whose equivalents cannot be found in the calculated spectrum; and 28.80–29.20 and 31.10–31.90 Å, which are regions with equally strong lines with separations approximately equal to the uncertainties expected in the FAC calculations.

The lines for which there is only one candidate transition are listed in Table I, while Table II lists lines for which more than one candidate is possible, or strong lines which are likely to belong to tungsten but have no clear candidates at all. Weak lines without any candidate transitions have not been listed. Each experimental wavelength inside a block in Table II is judged to be equally likely to correspond to any of the candidate transitions in the same block. The levels are denoted through the $jj$-coupling scheme, with the most dominating configuration given in the tables. Due to level mixing, some of the levels in our calculations have the same dominating configuration. In these cases, the level numbering as given by FAC is presented as well, with the ground level numbered as (1). Intermediate angular momenta are included when needed to avoid ambiguities in the designation, or for clarity.

There are a few earlier experimental studies with which to compare our measured wavelengths. The Co-like $W^{47+}$ line at 27.6821 Å was previously reported by Ekberg *et al.* [50], who arrived at a value of 27.671 Å by interpolation in the Co isoelectronic sequence. These two values differ by 11 mÅ, which is higher than the uncertainty of 5 mÅ as estimated by Ekberg *et al.* However, since the line was not directly observed in their work we assess the value reported in this paper to be more reliable. The Co-like $W^{47+}$ line at 27.6821 Å and the Fe-like $W^{48+}$ line at 27.5055 Å were observed by Seely *et al.* [51] in a laser-produced plasma. Their reported values of 27.668 and 27.520 Å, respectively, are consistent with this work within their estimated uncertainty of 15 mÅ.

A few of the transitions reported in this work share levels with previously reported transitions, making it

TABLE I. Observed W-ion transitions sorted by ion. All transitions are of $E1$ type, with exceptions noted in the line designation. When needed to avoid ambiguities, the FAC level number is given in parentheses.

| Key | $\lambda_{expt}$ (Å) | $\lambda_{prev}$ (Å) | $\lambda_{FAC}$ | Lower level | Upper level |
|---|---|---|---|---|---|
| Co-1 | 27.6821(7) | 27.671(5)[a] | 27.574 | $[(3p^6 3d^4_{3/2})_0\ 3d^5_{5/2}]_{5/2}$ | $[(3d^{10} 3p^2_{1/2})_0\ 3p^3_{3/2}]_{3/2}$ |
| | | 27.668(15)[b] | | | |
| | | 27.52[k] | | | |
| Co-2 | 32.532(3) | 32.533(1)[c] | 32.383 | $[(3p^6 3d^6_{5/2})_0\ 3d^3_{3/2}]_{3/2}$ | $[(3d^{10} 3p^2_{1/2})_0\ 3p^3_{3/2}]_{3/2}$ |
| | | 32.29[k] | | | |
| Fe-1 | 27.5055(9) | 27.520(15)[b] | 27.362 | $[(3p^6 3d^4_{3/2})_0\ 3d^4_{5/2}]_4$ | $[(3p^2_{1/2} 3p^3_{3/2} 3d^4_{3/2})_{3/2}\ 3d^5_{5/2}]_3$ |
| Mn-1 | 27.5702(7) | | 27.428 | $[(3p^6 3d^4_{3/2})_0\ 3d^3_{5/2}]_{9/2}$ | $[(3p^2_{1/2} 3p^3_{3/2} 3d^4_{3/2})_{3/2}\ (3d^4_{5/2})_4]_{7/2}$ |
| Cr-1 | 28.894(2) | | 28.796 | $[(3p^6 3d^4_{3/2})_0\ 3d^2_{5/2}]_4$ | $[(3p^2_{1/2} 3p^3_{3/2} 3d^4_{3/2})_{3/2}\ (3d^3_{5/2})_{9/2}]_4$ |
| V-1 | 29.124(1) | | 29.018 | $[(3p^6 3d^4_{3/2})_0\ 3d_{5/2}]_{5/2}$ | $[(3p^2_{1/2} 3p^3_{3/2} 3d^4_{3/2})_{3/2}\ (3d^2_{5/2})_4]_{5/2}$ |
| V-2 | 30.285(2) | | 30.260 | $[(3p^6 3d^4_{3/2})_0\ 3d_{5/2}]_{5/2}$ | $[(3p^2_{1/2} 3p^3_{3/2} 3d^4_{3/2})_{3/2}\ (3d^2_{5/2})_4]_{7/2}$ |
| V-3 | 31.997(1) | | 32.053 | $[(3p^6 3d^4_{3/2})_0\ 3d_{5/2}]_{5/2}$ | $[(3p^2_{1/2} 3p^3_{3/2} 3d^4_{3/2})_{3/2}\ (3d^2_{5/2})_2]_{7/2}$ |
| Ti-1 | 29.968(1) | | 29.860 | $[3p^6 3d^4_{3/2}]_0$ | $[(3p^2_{1/2} 3p^3_{3/2} 3d^4_{3/2})_{3/2}\ 3d_{5/2}]_1$ |
| Sc-1 | 30.181(2) | | 30.051 | $[3p^6 3d^3_{3/2}]_{3/2}$ | $[(3p^2_{1/2} 3p^3_{3/2} 3d^3_{3/2})_3\ 3d_{5/2}]_{3/2}$ |
| Sc-2 | 30.902(1) | | 30.813 | $[3p^6 3d^3_{3/2}]_{3/2}$ | $[(3p^2_{1/2} 3p^3_{3/2} 3d^3_{3/2})_2\ 3d_{5/2}]_{5/2}$ |
| Sc-3 | 31.379(2) | | 31.365 | $[3p^6 3d^3_{3/2}]_{3/2}$ | $[(3p^2_{1/2} 3p^3_{3/2} 3d^3_{3/2})_3\ 3d_{5/2}]_{1/2}$ |
| Ca-1 | 31.430(1) | | 31.386 | $[3p^6 3d^2_{3/2}]_2$ | $[((3p^2_{1/2} 3p^3_{3/2})_{3/2}\ (3d^2_{3/2})_0)_{3/2}\ 3d_{5/2}]_3$ |
| Ca-2 | 31.563(2) | | 31.505 | $[3p^6 3d^2_{3/2}]_2$ | $[((3p^2_{1/2} 3p^3_{3/2})_{3/2}\ (3d^2_{3/2})_2)_{5/2}\ 3d_{5/2}]_2$ |
| Ca-3 | 31.8110(9) | | 31.786 | $[3p^6 3d^2_{3/2}]_2$ | $[((3p^2_{1/2} 3p^3_{3/2})_{3/2}\ (3d^2_{3/2})_2)_{7/2}\ 3d_{5/2}]_1$ |
| K-1 | 32.403(1) | | 32.316 | $[3p^6 3d_{3/2}]_{3/2}$ | $[(3p^2_{1/2} 3p^3_{3/2} 3d_{3/2})_2\ 3d_{5/2}]_{5/2}$ |
| K-2 | 33.040(1) | | 33.015 | $[3p^6 3d_{3/2}]_{3/2}$ | $[(3p^2_{1/2} 3p^3_{3/2} 3d_{3/2})_3\ 3d_{5/2}]_{3/2}$ |
| Ar-1 | 33.340(5) | | 33.268 | $[(3p^2_{1/2} 3p^3_{3/2})_{3/2}\ 3d_{3/2}]_3$ | $[(3p^2_{1/2} 3p^2_{3/2})_0\ 3d_{3/2} 3d_{5/2}]_4$ (37) |
| Ar-2 | 33.541(1) | | 33.481 | $[3p^6]_0$ | $[3p^2_{1/2} 3p^3_{3/2} 3d_{5/2}]_1$ |
| Ar-3 | 34.277(5) | | 34.266 | $[(3p^2_{1/2} 3p^3_{3/2})_{3/2}\ 3d_{3/2}]_3$ | $[((3p^2_{1/2} 3p^2_{3/2})_2\ 3d_{3/2})_{7/2}\ 3d_{5/2}]_3$ |
| Cl-1 | 34.634(2) | 34.062[h] | 34.590 | $[3p^2_{1/2} 3p^3_{3/2}]_{3/2}$ | $[(3p^2_{1/2} 3p^2_{3/2})_2\ 3d_{5/2}]_{5/2}$ |
| Cl-2 | 35.043(1) | 34.478[h] | 34.997 | $[3p^2_{1/2} 3p^3_{3/2}]_{3/2}$ | $[(3p^2_{1/2} 3p^2_{3/2})_2\ 3d_{5/2}]_{3/2}$ |
| S-1 | 35.974(2) | 35.68[i] | 35.945 | $[3p^2_{1/2} 3p^2_{3/2}]_2$ | $[3p^2_{1/2} 3p_{3/2} 3d_{5/2}]_3$ |
| S-2 | 36.881(3) | 36.63[i] | 36.855 | $[3p^2_{1/2} 3p^2_{3/2}]_0$ | $[3p^2_{1/2} 3p_{3/2} 3d_{5/2}]_1$ |
| S-3 | 38.072(2) | 37.92[i] | 38.107 | $[3p^2_{1/2} 3p^2_{3/2}]_2$ | $[3p^2_{1/2} 3p_{3/2} 3d_{5/2}]_2$ |
| P-1$^{M1}$ | 35.109(2) | 35.10(1)[c] | 35.086 | $[3p^2_{1/2} 3p_{3/2}]_{3/2}$ | $[3p_{1/2}(3p^2_{3/2})_2]_{5/2}$ |
| | | 35.13[g] | | | |
| | | 35.08[j] | | | |
| P-2$^{M1}$ | 36.323(2) | 36.42[g] | 36.319 | $[3p^2_{1/2} 3p_{3/2}]_{3/2}$ | $[3p_{1/2}(3p^2_{3/2})_2]_{3/2}$ |
| | | 36.31[j] | | | |
| P-3 | 38.268(2) | 38.13[g] | 38.282 | $[3p^2_{1/2} 3p_{3/2}]_{3/2}$ | $[3p^2_{1/2} 3d_{5/2}]_{5/2}$ |
| Si-1$^{E2}$ | 34.720(1) | 34.760[f] | 34.699 | $[3p^2_{1/2}]_0$ | $[3p_{1/2} 3p_{3/2}]_2$ |
| | | 34.69[j] | | | |
| Si-2 | 37.12(1) | | 37.074 | $[3s_{1/2} 3p^2_{1/2} 3p_{3/2}]_2$ | $[3s_{1/2} 3p^2_{1/2} 3d_{5/2}]_2$ |
| Si-3 | 39.65(1) | 39.588[f] | 39.668 | $[3p_{1/2} 3p_{3/2}]_2$ | $[3p_{1/2} 3d_{5/2}]_3$ |
| Si-4 | 40.472(4) | | 40.466 | $[3s_{1/2} 3p^2_{1/2} 3p_{3/2}]_1$ | $[3s_{1/2} 3p^2_{1/2} 3d_{5/2}]_2$ |
| Al-1$^{M1}$ | 34.110(7) | 34.123[d] | 34.092 | $[3p_{1/2}]_{1/2}$ | $[3p_{3/2}]_{3/2}$ |
| | | 34.20[e] | | | |
| | | 34.08[j] | | | |
| Al-2 | 40.37(1) | 40.40[d] | 40.370 | $[3p_{3/2}]_{3/2}$ | $[3d_{5/2}]_{5/2}$ |
| | | 40.29[e] | | | |

[a]From Ekberg *et al.* [50].
[b]From Seely *et al.* [51].
[c]Inferred from earlier measurements by Ralchenko *et al.* [14,34].
[d]Inferred from RMBPT calculations by Safronova and Safronova [25].
[e]From the MCDF calculations by Huang [23].
[f]From the MCDF calculations by Huang [27].
[g]From the MCDF calculations by Huang [28].
[h]From the MCDF calculations by Huang *et al.* [30].
[i]From the MCDF calculations by Chou *et al.* [29].
[j]From calculations by Quinet [31].
[k]From the theoretical work by Fournier [32].

TABLE II. Observed spectral lines in W ions, sorted by wavelength with candidate transitions. All candidate transitions are of $E1$ type, with exceptions noted in the line designation. When needed to avoid ambiguities, the FAC level number is given in parentheses.

| $\lambda_{expt}$ (Å) | Ion | $\lambda_{FAC}$ (Å) | Lower level | Upper level |
|---|---|---|---|---|
| 27.781(4) | | | | |
| 27.856(3) | | | | |
| 28.010(3) | | | | |
| 28.067(3) | | | | |
| 28.1510(9) | Cr | 28.010 | $[(3p^6 3d^4_{3/2})_0\ 3d^2_{5/2}]_4$ | $[(3p^2_{1/2}3p^3_{3/2}3d^4_{3/2})_{3/2}\ (3d^3_{5/2})_{5/2}]_3$ (44) |
| 28.220(2) | Mn | 28.095 | $[(3p^6 3d^4_{3/2})_0\ 3d^3_{5/2}]_{5/2}$ | $[(3p^2_{1/2}3p^3_{3/2}3d^4_{3/2})_{3/2}\ (3d^4_{5/2})_2]_{3/2}$ |
| 28.243(1) | Cr | 28.444 | $[(3p^6 3d^4_{3/2})_0\ 3d^2_{5/2}]_2$ | $[(3p^2_{1/2}3p^3_{3/2}3d^4_{3/2})_{3/2}\ (3d^3_{5/2})_{3/2}]_2$ |
| 28.334(2) | Fe | 28.467 | $[(3p^6 3d^4_{3/2})_0\ 3d^4_{5/2}]_0$ | $[(3p^2_{1/2}3p^3_{3/2}3d^4_{3/2})_{3/2}\ 3d^5_{5/2}]_1$ |
| 28.558(2) | Cr | 28.504 | $[(3p^6 3d^4_{3/2})_0\ 3d^2_{5/2}]_2$ | $[(3p^2_{1/2}3p^3_{3/2}3d^4_{3/2})_{3/2}\ (3d^3_{5/2})_{5/2}]_3$ (44) |
| 28.583(2) | Mn | 28.511 | $[(3p^6 3d^4_{3/2})_0\ 3d^3_{5/2}]_{5/2}$ | $[(3p^2_{1/2}3p^3_{3/2}3d^4_{3/2})_{3/2}\ (3d^4_{5/2})_4]_{5/2}$ |
| 28.798(3) | | | | |
| 28.837(3) | | | | |
| 28.9910(8) | Fe | 28.967 | $[(3p^6 3d^4_{3/2})_0\ 3d^4_{5/2}]_2$ | $[(3p^2_{1/2}3p^3_{3/2}3d^4_{3/2})_{3/2}\ 3d^5_{5/2}]_2$ |
| 29.0360(8) | Fe | 29.044 | $[(3p^6 3d^4_{3/2})_0\ 3d^4_{5/2}]_4$ | $[(3p^2_{1/2}3p^3_{3/2}3d^4_{3/2})_{3/2}\ 3d^5_{5/2}]_4$ |
| | Mn | 29.051 | $[(3p^6 3d^4_{3/2})_0\ 3d^3_{5/2}]_{9/2}$ | $[(3p^2_{1/2}3p^3_{3/2}3d^4_{3/2})_{3/2}\ (3d^4_{5/2})_4]_{9/2}$ |
| 29.399(2) | V | 29.301 | $[(3p^6 3d^3_{3/2})_{3/2}\ (3d^2_{5/2})_4]_{11/2}$ | $[(3p^2_{1/2}3p^3_{3/2}3d^3_{3/2})_3\ (3d^3_{5/2})_{9/2}]_{11/2}$ |
| | Cr | 29.331 | $[(3p^6 3d^4_{3/2})_0\ 3d^2_{5/2}]_2$ | $[(3p^2_{1/2}3p^3_{3/2}3d^4_{3/2})_{3/2}\ (3d^3_{5/2})_{5/2}]_3$ (42) |
| | Ti | 29.415 | $[(3p^6 3d^3_{3/2})_{3/2}\ 3d_{5/2}]_3$ | $[(3p^2_{1/2}3p^3_{3/2}3d^3_{3/2})_3\ (3d^2_{5/2})_2]_2$ (73) |
| | Ca | 29.452 | $[3p^6 3d^2_{3/2}]_2$ | $[((3p^2_{1/2}3p^3_{3/2})_{3/2}\ (3d^2_{3/2})_0)_{3/2}\ 3d_{5/2}]_1$ |
| | Cr | 29.497 | $[(3p^6 3d^3_{3/2})_{3/2}\ (3d^3_{5/2})_{9/2}]_6$ | $[(3p^2_{1/2}3p^3_{3/2}3d^3_{3/2})_3\ (3d^4_{5/2})_4]_6$ |
| 29.560(2) | Ca | 29.452 | $[3p^6 3d^2_{3/2}]_2$ | $[((3p^2_{1/2}3p^3_{3/2})_{3/2}\ (3d^2_{3/2})_0)_{3/2}\ 3d_{5/2}]_1$ |
| | Cr | 29.497 | $[(3p^6 3d^3_{3/2})_{3/2}\ (3d^3_{5/2})_{9/2}]_6$ | $[(3p^2_{1/2}3p^3_{3/2}3d^3_{3/2})_3\ (3d^4_{5/2})_4]_6$ |
| | Ti | 29.654 | $[(3p^6 3d^3_{3/2})_{3/2}\ 3d_{5/2}]_3$ | $[(3p^2_{1/2}3p^3_{3/2}3d^3_{3/2})_2\ (3d^2_{5/2})_2]_3$ (71) |
| 29.615(1) | Ti | 29.654 | $[(3p^6 3d^3_{3/2})_{3/2}\ 3d_{5/2}]_3$ | $[(3p^2_{1/2}3p^3_{3/2}3d^3_{3/2})_2\ (3d^2_{5/2})_2]_3$ (71) |
| 29.864(3) | Cr | 29.800 | $[(3p^6 3d^4_{3/2})_0\ 3d^2_{5/2}]_2$ | $[(3p^2_{1/2}3p^3_{3/2}3d^4_{3/2})_{3/2}\ (3d^3_{5/2})_{5/2}]_2$ |
| 29.928(1) | | | | |
| 30.966(2) | Ti | 30.883 | $[(3p^6 3d^3_{3/2})_{3/2}\ 3d_{5/2}]_4$ | $[(3p^2_{1/2}3p^3_{3/2}3d^3_{3/2})_3\ (3d^2_{5/2})_4]_5$ |
| | Ti | 30.932 | $[(3p^6 3d^3_{3/2})_{3/2}\ 3d_{5/2}]_3$ | $[(3p^2_{1/2}3p^3_{3/2}3d^3_{3/2})_3\ (3d^2_{5/2})_4]_4$ |
| | Mn | 31.008 | $[(3p^6 3d^4_{3/2})_0\ 3d^3_{5/2}]_{5/2}$ | $[(3p^2_{1/2}3p^3_{3/2}3d^4_{3/2})_{3/2}\ (3d^4_{5/2})_2]_{7/2}$ |
| 31.245(3) | Ca | 31.155 | $[3p^6 3d^2_{3/2}]_0$ | $[((3p^2_{1/2}3p^3_{3/2})_{3/2}\ (3d^2_{3/2})_0)_{3/2}\ 3d_{5/2}]_1$ |
| 31.279(2) | Cr | 31.271 | $[(3p^6 3d^4_{3/2})_0\ 3d^2_{5/2}]_4$ | $[(3p^2_{1/2}3p^3_{3/2}3d^4_{3/2})_{3/2}\ (3d^3_{5/2})_{9/2}]_5$ |
| 31.749(1) | K | 31.669 | $[3p^6 3d_{3/2}]_{3/2}$ | $[((3p^2_{1/2}3p^3_{3/2})_{3/2}\ 3d_{3/2})_3\ 3d_{5/2}]_{1/2}$ |
| 31.776(3) | Ca | 31.711 | $[3p^6 3d^2_{3/2}]_2$ | $[((3p^2_{1/2}3p^3_{3/2})_{3/2}\ (3d^2_{3/2})_0)_{3/2}\ 3d_{5/2}]_3$ |
| 32.264(4) | Ti | 32.289 | $[(3p^6 3d^3_{3/2})_{3/2}\ 3d_{5/2}]_4$ | $[(3p^2_{1/2}3p^3_{3/2}3d^3_{3/2})_3\ (3d^2_{5/2})_2]_5$ |
| | Ca | 32.416 | $[3p^6 3d^2_{3/2}]_2$ | $[((3p^2_{1/2}3p^3_{3/2})_{3/2}\ (3d^2_{3/2})_0)_{3/2}\ 3d_{5/2}]_2$ |
| 34.779(4) | $S^{M1}$ | 34.735 | $[3p^2_{1/2}3p^2_{3/2}]_2$ | $[3p_{1/2}3p^3_{3/2}]_2$ |
| | S | 34.800 | $[3p^2_{1/2}3p^2_{3/2}]_2$ | $[3p^3_{3/2}3d_{5/2}]_1$ |
| | K | 34.812 | $[3p^6 3d_{3/2}]_{3/2}$ | $[((3p^2_{1/2}3p^3_{3/2})_{3/2}\ 3d_{3/2})_3\ 3d_{5/2}]_{5/2}$ |
| 35.668(4) | $Cl^{M1}$ | 35.635 | $[3p^2_{1/2}3p^3_{3/2}]_{3/2}$ | $[3p_{1/2}3p^4_{3/2}]_{1/2}$ |
| 35.644(4) | $Si^{M1}$ | 35.648 | $[3p^2_{1/2}]_0$ | $[3p_{1/2}3p_{3/2}]_1$ |
| | Cl | 35.672 | $[3p^2_{1/2}3p^3_{3/2}]_{3/2}$ | $[(3p^2_{1/2}3p^2_{3/2})_0\ 3d_{5/2}]_{5/2}$ |
| | $S^{M1}$ | 35.708 | $[3p^2_{1/2}3p^2_{3/2}]_2$ | $[3p_{1/2}3p^3_{3/2}]_1$ |

possible to indirectly compare our results with previous studies. By combining the $[(3p^6 3d^4_{3/2})_0\ 3d^5_{5/2}]_{5/2}$-$[(3p^6 3d^3_{3/2})_{3/2}3d^6_{5/2}]_{3/2}$ transition at 185.67 Å in Co-like $W^{47+}$ reported by Ralchenko *et al.* [14] with our Co-like $[(3p^6 3d^4_{3/2})_0\ 3d^5_{5/2}]_{5/2}$-$[(3d^{10}3p^2_{1/2})_0\ 3p^3_{3/2}]_{3/2}$ transition at 27.6821 Å, there will be an expected $[(3p^6 3d^6_{5/2})_0\ 3d^3_{3/2}]_{3/2}$-$[(3d^{10}3p^2_{1/2})_0\ 3p^3_{3/2}]_{3/2}$ transition at 32.533 Å, consistent with the line observed in this work at 32.532 Å. Similarly, by combining $[3p^2_{1/2}3p_{3/2}]_{3/2}$-$[3p^2_{1/2}3d_{3/2}]_{3/2}$ at 53.96 Å and $[3p^2_{1/2}3d_{3/2}]_{3/2}$-$[3p_{1/2}(3p^2_{3/2})_2]_{5/2}$ at 100.16 Å in

P-like $W^{59+}$ from Ralchenko *et al.* [34], a $[3p_{1/2}^2 3p_{3/2}]_{3/2}$-$[3p_{1/2}(3p_{3/2}^2)_2]_{5/2}$ transition at 35.10 Å can be inferred. This matches the line at 35.109 Å in this work, which might be blended with the $[3s_{1/2}3p_{3/2}]_1$-$[3s_{1/2}3p_{3/2}]_2$ transition in Mg-like $W^{62+}$, predicted by FAC to have a wavelength of 35.120 Å. However, the Mg-like line has likely a lower intensity than the P-like $W^{59+}$ line, and MCHF calculations on Mg-like systems by Zou and Froese Fischer [52] predict this transition to have an energy of 2 849 400 $cm^{-1}$, corresponding to 35.095 Å. Thus, the Mg-like transition might in fact be blended with the $1s^2$-$1s3p$ transition in C V at 34.97 Å.

Comparable wavelength data obtained from theoretical works are presented in Table I. Most wavelengths are taken directly from the data tables found in the papers, but in a few cases the transitions we have measured have not been explicitly calculated, even though values for the energy levels have been given. In these cases we have simply converted the energy differences to wavelength units. For instance, the RMBPT calculations on Al-like ions by Safronova and Safronova [25] give an energy difference between the $[3p_{1/2}]_{1/2}$ and $[3p_{3/2}]_{3/2}$ levels in $W^{61+}$ of 2 930 600 $cm^{-1}$. This corresponds to an expected transition of ∼34.123 Å, which fits well with the line observed at 34.110(7) Å.

The early MCDF calculations by Huang [27,28], Huang *et al.* [30], and Chou *et al.* [29] deviate strongly from our measurements. For instance, the lines designated as Cl-1 and Cl-2 in this work differ from the calculations by Huang *et al.* [30] by over 10 000 ppm. In more recent works by Safronova and Safronova [25] and Quinet [31], the difference is ∼300–1000 ppm. Since Quinet [31] focuses on $M1$ and $E2$ transitions between the lowest-lying energy levels in the ions investigated, it is possible to compare these wavelengths with ours only down to P-like $W^{59+}$. However, it is likely that the deviations increase for even lower charge states; if the values of Quinet [31] are compared with those measured by Ralchenko *et al.* [14] it can be concluded that the difference for the lowest charge states is typically several thousand ppm.

## IV. SUMMARY AND CONCLUSION

This paper reports on wavelengths for 35 identified $M$-shell transitions in highly charged multielectron tungsten ions in the 27–41 Å region. The lines have been found to originate from Al-like $W^{61+}$ through Co-like $W^{47+}$ by comparing the experimental line positions and intensities to theoretical spectra calculated by FAC. The wavelength uncertainties are typically below 100 ppm, with a number of lines in the 25–30 ppm range, which is very low and comparable with the 30 ppm uncertainty of the Ti-like $W^{51+}$ line measured in the visible part of the spectrum by Utter *et al.* [37]. Our measurements are found to be consistent with the few experimental studies previously published, typically with ten times higher precision.

The typical deviation between experimental and FAC wavelengths is a few hundred ppm for the highest charge states, while increasing to a few thousand ppm in systems with more electrons. Thus, the unaccounted correlation effects, increasing with the number of electrons, lead to bigger discrepancies with our measurements the lower the charge of the ion. The decrease of precision renders it difficult to identify every line in the spectrum, and 28 strong lines for which there are more than one candidate transition, or none, are also listed in this work. The most recent calculations by Safronova and Safronova [25], who used very sophisticated relativistic many-body perturbation theory, including the Breit interaction, and by Quinet [31], who used the fully relativistic multiconfiguration Dirac-Fock method, typically differ from our measurements by ∼300–1000 ppm. Theoretical data on Cl-like $W^{57+}$ and S-like $W^{58+}$ [29,30] may differ by over ∼10 000 ppm. Thus, the observed lines which have been identified should provide excellent opportunities for testing new high-precision structure codes designed for multielectron high-$Z$ ions.

In addition, it is important to note the plasma diagnostic potential of a few of the lines presented in this paper. According to our FAC calculations, the lowest-lying group of levels in the lower charge states are all states belonging to the $3p^6 3d^n$ configurations. Relatively strong $M1$ transitions within this group result in radiation in the 120–210 Å range, as shown through recent studies by Ralchenko *et al.* [14]. The subsequent excited group of configurations is $3p^5 d^{n+1}$, which typically is separated from the ground configurations by a gap of a few hundred eV, resulting in $3p^6 3d^n$-$3p^5 d^{n+1}$ $E1$ transitions well below 100 Å. In contrast, the lowest levels in the higher charge states with open $3p$ subshells are of several different configurations. For instance, the six lowest levels in P-like $W^{59+}$ are, in ascending order, $[3p_{1/2}^2 3p_{3/2}]_{3/2}$, $[3p_{1/2}^2 3d_{3/2}]_{3/2}$, $[3p_{1/2}^2 3d_{5/2}]_{5/2}$, and $[3p_{1/2}3p_{3/2}^2]_{3/2,\,5/2,\,1/2}$. As a consequence, $E1$ and $M1$ transitions between these levels fall, according to our FAC results, in the narrow range of ∼34–40 Å, with similar conditions applying to other ions with unfilled $3p$ subshells, such as Al-like $W^{61+}$ and Si-like $W^{60+}$. These transitions have been observed and are included in Table I together with a number of candidate high-order multipole transitions in Table II. The fact that both $E1$ and high-order multipole transitions are very close to each other in this region renders 34–40 Å a range with potential future use in electron-density measurements of fusion plasmas.

## ACKNOWLEDGMENTS

Work at Lawrence Livermore National Laboratory was performed under the auspices of the United States Department of Energy under Contract No. DE-AC52-07NA27344. The work was carried out as part of the Livermore WOLFRAM Project and the International Atomic Energy Agency (IAEA) Coordinated Research Project "Spectroscopic and Collisional Data for Tungsten from 1 eV to 20 keV." T.L. would like to acknowledge funding from Swedish Energy Agency Grant No. P3015-2.

[1] I. Martinson, Nucl. Instrum. Methods Phys. Res. B **43**, 323 (1989).
[2] J. D. Gillaspy, J. Phys. B **34**, R93 (2001).
[3] M. H. Chen and K. T. Cheng, J. Phys. B **43**, 074019 (2010).
[4] K. T. Cheng, M. H. Chen, W. R. Johnson, and J. Sapirstein, Can. J. Phys. **86**, 33 (2008).

[5] I. P. Grant, B. J. McKenzie, P. H. Norrington, D. F. Mayers, and N. C. Pyper, Comput. Phys. Commun. **21**, 207 (1980).
[6] B. J. McKenzie, I. P. Grant, and P. H. Norrington, Comput. Phys. Commun. **21**, 233 (1980).
[7] M. S. Safronova, W. R. Johnson, and U. I. Safronova, Phys. Rev. A **54**, 2850 (1996).
[8] U. I. Safronova, W. R. Johnson, and M. S. Safronova, At. Data Nucl. Data Tables **69**, 183 (1998).
[9] Y. Ishikawa, H. M. Quiney, and G. L. Malli, Phys. Rev. A **43**, 3270 (1991).
[10] Y. Ishikawa and M. J. Vilkas, Phys. Rev. A **63**, 042506 (2001).
[11] Y. Ralchenko, J. N. Tan, J. D. Gillaspy, J. M. Pomeroy, and E. Silver, Phys. Rev. A **74**, 042514 (2006).
[12] J. Clementson, P. Beiersdorfer, and M. F. Gu, Phys. Rev. A **81**, 012505 (2010).
[13] P. Beiersdorfer, J. K. Lepson, M. B. Schneider, and M. P. Bode, Phys. Rev. A **86**, 012509 (2012).
[14] Y. Ralchenko, I. N. Draganic, D. Osin, J. D. Gillaspy, and J. Reader, Phys. Rev. A **83**, 032517 (2011).
[15] E. Träbert, Phys. Scr., T **100**, 88 (2002).
[16] E. Träbert, Can. J. Phys. **86**, 73 (2008).
[17] N. J. Peacock, M. G. O'Mullane, R. Barnsley, and M. R. Tarbutt, Can. J. Phys. **86**, 277 (2008).
[18] C. H. Skinner, Phys. Scr., T **134**, 014022 (2009).
[19] P. Beiersdorfer, J. Clementson, J. Dunn, M. F. Gu, K. Morris, Y. Podpaly, E. Wang, M. Bitter, R. Feder, K. W. Hill, D. Johnson, and R. Barnsley, J. Phys. B **43**, 144008 (2010).
[20] C. Biedermann, R. Radtke, R. Seidel, and T. Pütterich, Phys. Scr., T **134**, 014026 (2009).
[21] T. Pütterich, R. Neu, R. Dux, A. D. Whiteford, M. G. O'Mullane, and the ASDEX Upgrade Team, Plasma Phys. Control. Fusion **50**, 085016 (2008).
[22] J. Clementson, Ph.D. thesis, Lund University, 2010.
[23] K. N. Huang, At. Data Nucl. Data Tables **34**, 1 (1986).
[24] U. I. Safronova, M. Sataka, J. R. Albritton, W. R. Johnson, and M. S. Safronova, At. Data Nucl. Data Tables **84**, 1 (2003).
[25] U. I. Safronova and A. S. Safronova, J. Phys. B **43**, 074026 (2010).
[26] M. H. Chen and K. T. Cheng, Phys. Rev. A **84**, 012513 (2011).
[27] K. N. Huang, At. Data Nucl. Data Tables **32**, 503 (1985).
[28] K. N. Huang, At. Data Nucl. Data Tables **30**, 313 (1984).
[29] H. S. Chou, J. Y. Chang, Y. H. Chang, and K. N. Huang, At. Data Nucl. Data Tables **62**, 77 (1996).
[30] K. N. Huang, Y. K. Kim, K. T. Cheng, and J. P. Desclaux, At. Data Nucl. Data Tables **28**, 355 (1983).
[31] P. Quinet, J. Phys. B **44**, 195007 (2011).
[32] K. B. Fournier, At. Data Nucl. Data Tables **68**, 1 (1998).
[33] J. Clementson, P. Beiersdorfer, T. Bragge, and M. F. Gu (unpublished).
[34] Y. Ralchenko, I. N. Draganic, J. N. Tan, J. D. Gillaspy, J. M. Pomeroy, J. Reader, U. Feldman, and G. E. Holland, J. Phys. B **41**, 021003 (2008).
[35] J. Clementson and P. Beiersdorfer, Phys. Rev. A **81**, 052509 (2010).
[36] J. Clementson, P. Beiersdorfer, G. V. Brown, and M. F. Gu, Phys. Scr. **81**, 015301 (2010).
[37] S. B. Utter, P. Beiersdorfer, and G. V. Brown, Phys. Rev. A **61**, 030503(R) (2000).
[38] M. F. Gu, in *Atomic Processes in Plasmas*, edited by J. S. Cohen, S. Mazevet, and D. P. Kilcrease, AIP Conf. Proc. No. 730 (AIP, New York, 2004), p. 127.
[39] M. F. Gu, Can. J. Phys. **86**, 675 (2008).
[40] M. A. Levine, R. E. Marrs, J. N. Bardsley, P. Beiersdorfer, C. L. Bennett, M. H. Chen, T. Cowan, D. Dietrich, J. R. Henderson, D. A. Knapp, A. Osterheld, B. M. Penetrante, M. B. Schneider, and J. H. Scofield, Nucl. Instrum. Methods Phys. Res. B **43**, 431 (1989).
[41] P. Beiersdorfer, Can. J. Phys. **86**, 1 (2008).
[42] P. Beiersdorfer, E. W. Magee, E. Träbert, H. Chen, J. K. Lepson, M.-F. Gu, and M. Schmidt, Rev. Sci. Instrum. **75**, 3723 (2004).
[43] J. D. Garcia and J. E. Mack, J. Opt. Soc. Am. **55**, 654 (1965).
[44] G. W. Drake, Can. J. Phys. **66**, 586 (1988).
[45] L. A. Vainshtein and U. I. Safronova, Phys. Scr. **31**, 519 (1985).
[46] L. Engström and U. Litzén, J. Phys. B **28**, 2565 (1995).
[47] P. Beiersdorfer, A. L. Osterheld, M. H. Chen, J. R. Henderson, D. A. Knapp, M. A. Levine, R. E. Marrs, K. J. Reed, M. B. Schneider, and D. A. Vogel, Phys. Rev. Lett. **65**, 1995 (1990).
[48] R. E. Marrs, Can. J. Phys. **86**, 11 (2008).
[49] P. J. Mohr, B. N. Taylor, and D. B. Newell, Rev. Mod. Pys. **84**, 1527 (2012).
[50] J. O. Ekberg, U. Feldman, J. F. Seely, and C. M. Brown, J. Opt. Soc. Am. B **4**, 1913 (1987).
[51] J. F. Seely, C. M. Brown, and W. E. Behring, J. Opt. Soc. Am. B **6**, 3 (1989).
[52] Y. Zou and C. Froese Fischer, J. Phys. B **34**, 915 (2001).